Rational Attempts to Optimize Non-Natural Nucleotides for Selective Incorporation Opposite an Abasic Site†

Xuemei Zhang,§ Alison Donnelly,‡ Irene Lee,§ and Anthony J. Berdis*,‡

Departments of Pharmacology and Chemistry, Case Western Reserve University, 10900 Euclid Avenue, Cleveland, Ohio 44106

Received March 2, 2006; Revised Manuscript Received August 21, 2006

ABSTRACT: Translesion DNA synthesis represents the ability of a DNA polymerase to misinsert a nucleotide opposite a DNA lesion. Previous kinetic studies of the bacteriophage T4 DNA polymerase using a series of non-natural nucleotides suggest that π-electron density of the incoming nucleotide substantially contributes to the efficiency of incorporation opposite an abasic site, a nontemplating DNA lesion. However, it is surprising that these nonhydrogen-bonding analogues can also be incorporated opposite natural templating DNA with variable degrees of efficiency. In this article, we describe attempts to achieve selectivity for incorporation opposite the abasic site through optimization of π-electron density and shape of the nucleobase. Toward this goal, we report the synthesis and enzymatic characterization of two novel nucleotide analogues, 5-napthyl-indolyl-2′-deoxyriboside triphosphate (5-NapITP) and 5-anthracene-indolyl-2′-deoxyriboside triphosphate (5-AnITP). The overall catalytic efficiency for their incorporation opposite an abasic site is similar to that of other non-natural nucleotides such as 5-NITP and 5-PhITP that contain significant π-electron density. As expected, the incorporation of either 5-NapITP or 5-AnITP opposite templating DNA is reduced and presumably reflects steric constraints imposed by the large size of the polycyclic aromatic moieties. Furthermore, 5-NapITP is a chain terminator of translesion DNA synthesis because the DNA polymerase is unable to extend beyond the incorporated non-natural nucleotide. In addition, idle turnover measurements confirm that 5-NapIMP is stably incorporated opposite damaged DNA, and this enhancement reflects the overall favorable incorporation kinetic parameters coupled with a reduction in excision by the exonuclease-proofreading activity of the enzyme. On the basis of these data, we provide a comprehensive assessment of the potential role of π-electron surface area for nucleotide incorporation opposite templating and nontemplating DNA catalyzed by the bacteriophage T4 DNA polymerase.

The central dogma of replication fidelity is that the DNA polymerase utilizes the hydrogen-bonding potential of the templating nucleobase to guide the correct incorporation of its complementary partner. Although it is clear that proper hydrogen-bonding interactions play an important role in fidelity, there are instances where efficient polymerization occurs despite various modifications to these hydrogen-bonding functional groups (*1*−*6*). Of biological importance is the ability of DNA polymerases to misinsert and extend beyond damaged DNA because this activity can cause diseases including cancer, which are associated with mutagenesis. Indeed, there are numerous reports documenting the causal relationship between dysfunctional polymerase fidelity and cancer initiation (*7*−*11*).

Despite the obvious link between cancer and aberrant DNA replication, there are few reports documenting a valid strategy to prevent mutagenesis caused by inaccurate DNA synthesis (*12*, *13*). Reasons for this disparity include the wide variety of DNA lesions caused by DNA-damaging agents (*14*) and a lack of molecular details accounting for their replication. We previously proposed a strategy to inhibit the formation of genomic errors through the use of non-natural nucleotide analogues that could be selectively incorporated opposite damaged DNA to prevent their propagation (*13*). Our studies have focused on an apurinic/apyrimidinic (abasic) site that is highly pro-mutagenic because of its nontemplating nature (*15*−*17*). In addition, this lesion is commonly formed after the administration of chemotherapeutic agents such as cyclophosphamide (*18*) and temozolomide (*19*). Depurination by these types of alkylating agents can occur through the assistance of various DNA glycosylases or through nonenzymatic hydrolysis of the destabilized glycosidic bond (*20*). In fact, a major concern of chemotherapy is the generation of mutational errors caused by the inappropriate replication of unrepaired DNA lesions caused by these types of agents. It is now recognized that secondary cancers can develop as a result of inadvertent mutagenesis caused by DNA-damaging agents (*21*).

Despite the lack of coding information at an abasic site, we demonstrated that the bacteriophage T4 DNA polymerase, gp43, preferentially incorporates dATP opposite this lesion (*22*). This kinetic phenomenon, commonly referred to as the A-rule, is not unique to the bacteriophage polymerase because several other DNA polymerases, such as eukaryotic

† This research was supported through funding from the National Institutes of Health to A.J.B. (CA118408).

* Corresponding author. Tel: (216) 368-4723. Fax: (216) 368-3395. E-mail: ajb15@case.edu.

‡ Department of Pharmacology.

§ Department of Chemistry.

10.1021/bi060418v CCC: $33.50
Published on Web 10/12/2006

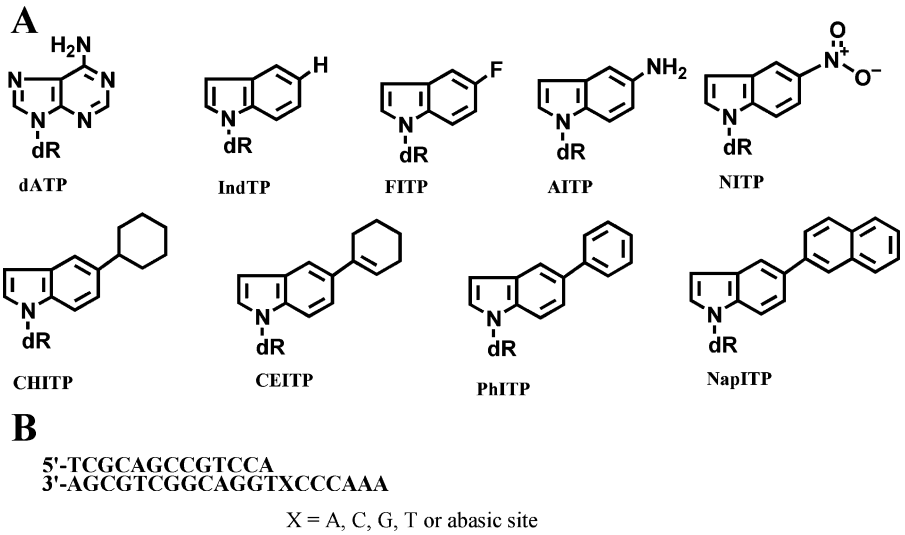

FIGURE 1: (A) Structures of 2′-deoxynucleoside triphosphates used or referred to in this study. For convenience, dR is used to represent the deoxyribose triphosphate portion of the nucleotides. (B) Defined DNA substrates used for kinetic analysis. The X in the template strand denotes any of the four natural nucleobases or the presence of a tetrahydrofuran moiety designed to functionally mimic an abasic site.

pol α (*23*), the Klenow fragment of *E. coli* (*24*), and HIV reverse transcriptase (*25*), also preferentially utilize dATP. However, the A-rule is not universal as certain polymerases such as pol iota preferentially incorporate dGTP opposite this lesion (*26*), whereas Rev1 prefers to incorporate dCTP (*27*). Regardless, we have used gp43 as a model to define the molecular features underlying this kinetic phenomenon for a high fidelity DNA polymerase. The strategy we have employed is to use a library of non-natural nucleotides that differ with respect to shape/size, solvation energies, dipole moment, and π-electron surface area (Figure 1A). Our studies were to first identify 5-NITP[1] as a unique nucleotide analogue possessing unprecedented kinetic behavior because it is incorporated with nearly a 1000-fold higher efficiency opposite an abasic site than dATP (*28*). Although 5-NITP binds with relatively high affinity ($K_D = 18\ \mu M$), the higher catalytic efficiency arises from a fast polymerization rate constant (k_{pol}) of 126 s^{-1}. Despite the extraordinary efficiency for incorporation opposite an abasic site, 5-NITP unfortunately suffers from a lack of selectivity because it is also incorporated opposite templating DNA with modest catalytic efficiency ($\sim 10^5\ M^{-1}\ s^{-1}$) (*28*).

We attempted to optimize the catalytic efficiency for incorporation opposite this DNA lesion by varying the degree of π-electron surface area at the 5-position of the indolyl-triphosphate (*29*, *30*). These attempts were initially successful because larger analogues that contain π-electron density such as 5-PhITP and 5-CE-ITP are incorporated opposite an abasic site with nearly identical catalytic efficiencies compared to those of 5-NITP (*29*, *30*). More importantly, both analogues are incorporated opposite templating DNA with average 10-fold lower catalytic efficiencies compared to those of 5-NITP (*29*, *30*).[2]

These data lead to the hypothesis that selectivity for incorporation opposite an abasic site could be achieved by balancing the contributions of π-electron surface area with the relative size of the nucleobase. In this design, the kinetics for incorporation opposite an abasic site could be enhanced if the incoming nucleotide contains a large enough π-electron surface area to stack favorably into the void created at the DNA lesion. In addition, the rate for incorporation opposite templating DNA would be reduced if the size of the 5-substituent group is sufficiently large enough to sterically clash with the templating nucleobase. Thus, a truly selective analogue for translesion synthesis could be developed by maximizing the catalytic efficiency for incorporation opposite an abasic site while restricting its incorporation opposite templating DNA.

To test this hypothesis, we synthesized two analogues, 5-napthyl-indolyl-2′-deoxyriboside triphosphate (5-NapITP) and 5-anthracene-indolyl-2′-deoxyriboside triphosphate (5-AnITP), which contain highly conjugated aromatic systems yet differ with respect to size. The kinetic data indicate that the catalytic efficiency for 5-NapITP incorporation opposite an abasic site is nearly identical to that measured using smaller analogues such as 5-NITP and 5-PhITP. In contrast, the larger analogue, 5-AnITP, shows a ~13-fold reduction in catalytic efficiency and argues that geometrical constraints imposed by the active site of the polymerase play an important role in limiting the rates of incorporation during translesion DNA synthesis. Regardless, both analogues are

[1] Abbreviations: TBE, Tris-HCl/borate/EDTA; EDTA; ethylenediaminetetraacetate, sodium salt; dNTP, deoxynucleoside triphosphate; dXTP, non-natural deoxynucleoside triphosphate; 5-NITP, 5-nitroindolyl-2′deoxyriboside triphosphate; 5-NapITP, 5-napthyl-indolyl-2′deoxyriboside triphosphate; 5-AnITP, 5-anthracene-indolyl-2′deoxyriboside triphosphate; 5-PhITP, 5-phenyl-indolyl-2′-deoxyriboside triphosphate; 5-CE-ITP, 5-cyclohexene-indolyl-2′deoxyriboside triphosphate; 5-CH-ITP, 5-cyclohexyl-indolyl-2′deoxyriboside triphosphate; gp43 exo$^-$, an exonuclease-deficient mutant of the bacteriophage T4 DNA polymerase; gp43 exo$^+$, wild-type bacteriophage T4 DNA polymerase.

[2] The average catalytic efficiency for 5-NITP incorporation opposite templating DNA was calculated to be $11 \times 10^4\ M^{-1}\ s^{-1}$ using the following values: $A = 1.91 \times 10^5\ M^{-1}\ s^{-1}$, $C = 3.61 \times 10^3\ M^{-1}\ s^{-1}$, $G = 1.20 \times 10^4\ M^{-1}\ s^{-1}$, and $T = 1.91 \times 10^5\ M^{-1}\ s^{-1}$ (*28*). The average catalytic efficiency for 5-PhITP incorporation opposite DNA was calculated to be $9.7 \times 10^3\ M^{-1}\ s^{-1}$ using the following values: $A = 4.0 \times 10^3\ M^{-1}\ s^{-1}$, $C = 6.8 \times 10^3\ M^{-1}\ s^{-1}$, $G = 2.17 \times 10^4\ M^{-1}\ s^{-1}$, and $T = 6.4 \times 10^3\ M^{-1}\ s^{-1}$ (*29*). The average catalytic efficiency for 5-CE-ITP incorporation opposite DNA was calculated to be $6.8 \times 10^3\ M^{-1}\ s^{-1}$ using the following values: $A = 4.8 \times 10^3\ M^{-1}\ s^{-1}$, $C = 2.0 \times 10^4\ M^{-1}\ s^{-1}$, $G = 1.2 \times 10^3\ M^{-1}\ s^{-1}$, and $T = 1.1 \times 10^3\ M^{-1}\ s^{-1}$ (*30*).

more effectively incorporated opposite an abasic site compared to incorporation opposite templating DNA. These results suggest that selectivity may be maintained through a negative selection mechanism. In addition, we provide a thorough characterization of the ability of the enzyme to extend and excise 5-NapIMP after incorporation opposite an abasic site. The reduction in degradation highlights the importance of base-stacking contributions toward hindering the activity of exonuclease proofreading.

MATERIALS AND METHODS

Materials. [γ-^{32}P]ATP was purchased from M.P. Biomedical (Irvine, CA). Unlabeled dNTPs (ultrapure) were obtained from Pharmacia. MgAcetate and Trizma base were from Sigma. Urea, acrylamide, and bis-acrylamide were from Aldrich. Oligonucleotides, including those containing a tetrahydrofuran moiety mimicking an abasic site, were synthesized by Operon Technologies (Alameda, CA). Single-stranded and duplex DNA were purified and quantified as described (*31*). All other materials were obtained from commercial sources and were of the highest quality available. The exonuclease-deficient mutant of gp43 (Asp-219 to Ala mutation) was purified and quantified as previously described (*32*, *33*).

Tributyl ammonium pyrophosphate was purchased from Sigma. 1-Chloro-2-deoxy-3,5-di-*O*-*p*-toluoyl-α-D-*erythro*-pentofuranose, ethyl acetate, hexane, methanol, dichloromethane, phosphoryl oxychloride, dimethyl formamide, and tributylamine were purchased from ACROS. Trimethyl phosphate and tributylamine were dried over 4 Å molecular sieves. DMF was distilled over ninhydrin and stored in 4 Å molecular sieves.

All NMR spectra were recorded in a Gemini-300 FT NMR spectrometer. Proton chemical shifts are reported in ppm, downfield from tetramethylsilane. Coupling constants (*J*) are reported in hertz (Hz). ^{31}P NMR spectra were taken in D_2O in the presence of 50 mM Tris (pH 7.5) and 2 mM EDTA, and 85% phosphoric acid was used as the external standard. Ultraviolet quantification of triphosphate was performed on Beckman DU-70. High-resolution electrospray mass spec (negative) was performed on Ionspec HiRES ESI-FTICRMS at the University of Cincinnati.

Synthesis of 5-Napthyl-indole 2′-deoxyribofuranoside 5′-triphosphate (5-NapITP). 5-Napthylindole was synthesized from bromo-napthalene and indole boric acid through a Suzuki coupling reaction (*34*). 1-(2-Deoxy-β-D-*erythro*pentafuranosyl)-5-napthyl-indole was prepared through glycosylation as previously described (*35*). The overall yield of the reaction was 70%. 1-(2-Deoxy-β-D-*erythro*pentafuranosyl)-5-napthyl-indole triphosphate (5-NapITP) was prepared starting with 5-napthyl indole-2′-deoxynucleoside. To a stirred and cooled (0 °C) solution of 5-napthyl-indole-2′-deoxynucleoside (20 mg, 0.055 mmol) and Et_3N (56 mg, 10 equiv, 0.55 mmol) in trimethyl phosphate (0.37 mL) was added dropwise phosphoryl oxychloride (7 μL, 1.5 equiv, 0.08 mmol). The mixture was simultaneously treated with a 0.5 M DMF solution of tributyl ammonium pyrophosphate (300 mg, 0.55 mmol) and tributylamine (0.09 mL, 0.38 mmol). After stirring the reaction mixture at room temperature for 15 min, it was neutralized with 1.0 M TEAB (15 mL). The reaction mixture was stirred at room temperature for 2 h, and was evaporated under reduced pressure at 32 °C to about 2 mL. The residue was purified by preparative reverse phase HPLC (300 pore size C-18 column from Vydac, 22 mm × 250 mm) with mobile phase buffer A: 0.1 M TEAB; and buffer B: 50% ACN in 0.1 M TEAB, using a linear gradient from 50% to 85% B within 18 min at a flow rate of 20.0 mL/min. The product was collected at 11.46 retention time and freeze-dried over night. The residue was stored in 10 mM TrisHCl at pH 7.5. The concentration was determined using an extinction coefficient of 53 087 M^{-1} cm^{-1} for the nucleoside.

5-Napthyl-indole H NMR ($CDCl_3$): 6.66 (1H, m, 3-H), 7.26(1H, m, 2-H), 7.45−7.65 (5H, m, Ar), 7.80−7.95 (3H, m, Ar), 8.00 (1H, s, Ar), 8.09 (1H, s, Ar), 8.22 (1H, br, NH) MS (+): calculated mass spec (formula $C_{18}H_{13}N$ for M + 1): 244. Experimental mass spec: 244. 1-(2′-Deoxy-β-D-*erythro*pentafuranosyl)-5-napthyl-indole H NMR (DMSO): 2.25 (1H, m, 2′-H), 2.45 (1H, m, 2′-H), 3.50 (2H, m, 5′-H), 3.85 (1H, m, 4′-H), 4.35 (1H, m, 3′-H), 4.90(1H, t, J = 3 Hz, 5′-OH), 5.30 (1H, d, J = 4 Hz, 3′-OH), 6.45 (1H, t, J = 6 Hz, 1′-H), 6.60 (1H, d, J = 3 Hz, 3-H), 7.45−7.50 (2H, m, Ar), 7.55−7.65 (4H, m, Ar), 7.80−8.05 (4H, m, Ar), 8.20 (1H, s, Ar).u.v. (MeOH) λ_{max} (nm) 254 (ϵ = 53 087) MS (+): calculated mass spec (formula: $C_{23}H_{22}NO_3$ for M + 1): 360. Experimental mass spec: 360. 1-(2′-Deoxy-β-D-*erythro*pentafuranosyl)-5-napthyl-indole triphosphate (5-NapITP): yield: 20%. H NMR (D_2O): 2.35 (1H, m, 2′-H), 2.75 (1H, m, 2′-H), 4.05 (2H, m, 5′-H), 4.15 (1H, m, 4′-H), 6.45 (1H, t, J = 6 Hz, 1′-H), 6.67 (1H, d, J = 3.4 Hz, 3-H), 7.45−8.10 (11H, m, Ar).^{31}P NMR (ppm) (D_2O/Tris): γ-P, −9.50 (d); α-P, −10.83 (d); β-P, −21.64 (t). HiRes ESI-MS (-): calculated mass spec (formula $C_{23}H_{23}NO_{12}P_3$ for M−H): 598.0433. Experimental mass spec: 598.0403.

Synthesis of 5-Anthracene-indole 2′-deoxyribofuranoside 5′-triphosphate (5-AnITP). Synthesis of 5-anthracenylindole triphosphate was started from 2-bromoanthracene (Astatech, Inc.) using the same method as that described for the 5-naphthylindole triphosphate. The final triphosphate was purified on preparative HPLC using conditions identical to those for 5-NapITP. The product was collected at a 17.11 min retention time and freeze-dried over night. The residue was stored in 10 mM TrisHCl at pH 7.5. The concentration is determined using the extinction coefficient (94 867 M^{-1} cm^{-1}) for the nucleoside.

5-Anthracenyl-indole H NMR ($CDCl_3$): 6.65 (1H, m, 3-H), 7.25−7.70 (5H, m, Ar), 7.85−8.10 (3H, m, Ar), 8.20 (1H, s, Ar), 8.25 (1H, br, NH) 8.40 (1H, s, Ar), 8.45 (1H, s, Ar). 1-(2′-Deoxy-β-D-*erythro*pentafuranosyl)-5-anthracenyl-indole: yield: 20% for two steps. H NMR (DMSO): 2.25 (1H, m, 2′-H), 2.45 (1H, m, 2′-H), 3.55 (2H, m, 5′-H), 3.85 (1H, m, 4′-H), 4.35 (1H, m, 3′-H), 4.90(1H, m, 5′-OH), 5.30 (1H, m, 3′-OH), 6.45 (1H, t, J = 6 Hz, 1′-H), 6.60 (1H, m, 3-H), 7.45−7.50 (2H, m, Ar), 7.65−7.75 (3H, m, Ar), 7.90 (1H, d, J = 7 Hz, Ar), 8.00−8.10 (3H, m, Ar), 8.20 (1H, d, J = 7 Hz, Ar), 8.35 (1H, s, Ar), 8.55 (1H, s, Ar), 8.62 (1H, s, Ar). UV (ethyl phosphate ester) λ_{max} (nm) 262 (ϵ = 94,-867), 274. MS (+): calculated mass spec (formula $C_{27}H_{23}NO_3$ for M): 409.1678. Experimental mass spec: 409.1688. 1-(2′-Deoxy-β-D-*erythro*pentafuranosyl)-5-anthracenyl-indole triphosphate (5-AntITP): yield: 5%. H NMR (D_2O): 2.30 (1H, m, 2′-H), 2.65 (1H, m, 2′-H), 4.00 (2H, m, 5′-H), 4.10 (1H, m, 4′-H), 6.40 (1H, t, J = 6 Hz, 1′-H), 6.60 (1H,

d, $J = 3.4$ Hz, 3-H), 7.35 (2H, m, Ar) 7.55 (1H, d, $J = 3.4$ Hz, Ar) 7.55 (2H, m, Ar), 8.20 (1H, s, Ar) 7.75 (1H, d, $J = 7$ Hz, Ar) 7.90−7.97 (3H, m, Ar), 8.00 (1H, d, $J = 7$ Hz, Ar) 8.40 (1H, s, Ar), 8.45(1H, s, Ar).^{31}P NMR (ppm) (D_2O/Tris): γ-P, −10,12 (d); α-P, −11.00 (d); β-P, −22.88 (t). HiRes ESI-MS (-): calculated mass spec (formula $C_{27}H_{25}NO_{12}P_3$ for M−H): 648.0590. Experimental mass spec: 648.0566.

Enzyme Assays. The assay buffer used in all kinetic studies consisted of 25 mM Tris-OAc (pH 7.5), 150 mM KOAc, and 10 mM 2-mercaptoethanol. All assays were performed at 25 °C. Polymerization reactions were monitored by analysis of the products on 20% sequencing gels as previously described (*31*). Gel images were obtained with a Packard PhosphorImager using the OptiQuant software supplied by the manufacturer. Product formation was quantified by measuring the ratio of ^{32}P-labeled extended and nonextended primer. The ratios of product formation are corrected for the substrate in the absence of polymerase (zero point). Corrected ratios are then multiplied by the concentration of primer/template used in each assay to yield the total product. All concentrations are listed as final solution concentrations.

Pre-Steady-State Nucleotide Incorporation Assays. A rapid quench instrument (KinTek Corporation, Clarence, PA) was used to monitor the time course in 5-NapITP incorporation. Experiments were performed using single turnover reaction conditions in which 500 nM gp43 exo$^-$ was incubated with 250 nM DNA in an assay buffer containing EDTA (100 μM) and mixed with variable concentrations of the nucleotide analogue (5 − 500 μM) and 10 mM $Mg(OAc)_2$. The reactions were quenched with 350 mM EDTA at variable times (0.005−10 s) and analyzed as described above. Data obtained for single turnover DNA polymerization assays were fit to eq 1.

$$y = A(1 - e^{-kt}) + C \quad (1)$$

where A is the burst amplitude, k is the observed rate constant (k_{obs}) in initial product formation, t is time, and C is a defined constant. Data for the dependency of k_{obs} as a function of dNTP concentration was fit to the Michaelis−Menten equation (eq 2) to provide values corresponding to k_{pol} and K_D.

$$k_{obs} = k_{pol}[dXTP]/(K_D + [dXTP]) \quad (2)$$

where k_{obs} is the observed rate constant of the reaction, k_{pol} is the maximal polymerization rate constant, K_D is the dissociation constant for dXTP, and dXTP is the concentration of non-natural nucleotide substrate.

Competition Experiments for Extension beyond an Abasic Site. Extension beyond an abasic site was performed under single turnover conditions using DNA containing an abasic site at the 14 position on the template (Figure 1B). DNA (250 nM) was incubated in assay buffer with 10 mM $Mg(OAc)_2$, 500 μM dATP, and 1000 μM dGTP in the presence or absence of 25 μM 5-NapITP. The reaction was initiated with 1 μM gp43 exo$^-$. The reactions were quenched with 200 mM EDTA at variable times (15−300 s) and analyzed as described above.

Pre-Steady-State Exonuclease Assays. A rapid quench instrument was used to monitor the time course in the hydrolysis of DNA containing 5-napthyl-indolyl-2′deoxyriboside in the primer strand. DNA was either single-stranded (14Nap-mer) or duplex DNA (14Nap/20SP-mer). In both cases, the 14Nap-mer was made by the enzymatic extension of the 13-mer using 5-Nap-ITP and terminal deoxynucleotidyl transferase (TdTase) using the manufacturer's protocols (Invitrogen). Briefly, 500 pmol of the 13-mer was reacted with 1 μL of TdTase and 100 μM 5-NapITP in a total reaction volume of 75 μL for 20 min at 37 °C. The reaction was quenched by heating at 65 °C for 10 min. The extended DNA was then purified using a G25-sephadex spin column to remove buffers used in the reaction with TdTase. Following purification, the DNA was radiolabeled with γ-^{32}P-ATP using T4 DNA polynucleotide kinase using the protocols supplied by the manufacturer (Invitrogen). A small aliquot of reaction product was analyzed by 20% sequencing gels as described (*31*) to validate that >95% of the original 13-mer was elongated to the corresponding 14Nap-mer (data not shown). In some experiments, the 14Nap-mer was used in the form of single-stranded DNA, whereas in other cases, the 14Nap-mer was annealed with an equimolar amount of the 20SP-mer to create the corresponding duplex (14Nap/20SP-mer). In all rapid quench experiments, a preincubated solution of 1 μM gp43 exo$^+$/10 mM Mg^{2+} was mixed versus 250 nM 5′-labeled DNA (final concentrations). The reaction was then terminated at various times by the addition of 350 mM EDTA, and the reaction products were analyzed as described above. The data points were plotted as initial substrate (typically the 14-mer) remaining as a function of time. Data for each time course were fit to eq 3, defining a first-order decay in initial substrate concentration.

$$y = Ae^{-kt} + C \quad (3)$$

where A is the amplitude of the burst phase, k is the observed rate constant for product formation, and C is the end point of the reaction.

Idle-Turnover Measurements. DNA (250 nM) (13/20SP-mer or 13/20T-mer) was first preincubated with variable concentrations of 5-NapITP (5−20 μM) or 5-PhITP (20 μM) in the presence of 30 μM dATP. Because of the nature of the DNA substrate (Figure 1B), the insertion of dAMP opposite T at position 13 in the template maintains a usable primer template for the insertion of the non-natural nucleotide opposite the abasic lesion (position 14). In all cases, the reaction was initiated through the addition of 1 μM gp43 exo$^+$. Then, 5 μL aliquots of the reaction were quenched into tubes containing 5 μL of 200 mM EDTA at times ranging from 5 to 300 s. The quenched samples were processed as described above, and product formation was analyzed using established protocols (*13*). Simulations modeling the observed kinetic time courses for nucleotide insertion and excision were performed by mathematical analyses using KINSIM (*35*) as previously described (*13*).

RESULTS AND DISCUSSION

The goal of this article was to rationally design non-natural nucleotides to be effectively incorporated opposite damaged DNA and poorly incorporated opposite normal templating DNA. Up till now, the unpredictable nature of most DNA

adducts has hindered the ability to design nucleotides that selectively target pro-mutagenic DNA synthesis. However, our previous mechanistic studies characterizing the incorporation of various non-natural nucleotide analogues opposite an abasic site (*13*, *28*−*30*) have provided insight into which biophysical feature of the nucleotide plays an important role. These studies demonstrate that analogues containing π-electron density, such as 5-NITP, 5-PhITP, and 5-CE-ITP, are efficiently incorporated opposite an abasic site ($k_{pol}/K_D \sim 5 \times 10^6$ M^{-1} s^{-1}). Unfortunately, these analogues suffer from relatively low selectivity because they were incorporated opposite undamaged DNA with modest catalytic efficiencies ($k_{pol}/K_D \sim 0.1-1 \times 10^4$ M^{-1} s^{-1}). It was noted, however, that the larger phenyl-indolyl and cyclohexene indolyl analogues are at least 10-fold more selective for translesion DNA synthesis than the smaller 5-nitro-indolyl nucleotide. This difference in selectivity suggests that discrimination could be influenced by manipulating the relative size of the substituent group at the 5-position of the indole. To test this hypothesis, we synthesized 5-NapITP and 5-AnITP in an attempt to optimize the contributions of shape/size and π-electron density, which are proposed to provide selective incorporation opposite an abasic site. The enzymatic characterization of these novel nucleotide analogues is provided below.

Measurements of k_{pol} and K_D for Incorporation Opposite an Abasic Site. K_D and k_{pol} values were measured for 5-NapITP and 5-AnITP incorporation opposite an abasic site to further define the role of π-electron surface area on the dynamics of translesion DNA synthesis. Experiments were performed using single turnover reaction conditions in which 1 μM gp43 exo$^-$ was incubated with 250 nM 13/20SP-mer and mixed with variable concentrations of 5-NapITP (5 − 80 μM) and 10 mM Mg^{2+}. Representative time courses provided in Figure 2A were fit to the equation for a single-exponential process to define k_{obs}, the rate constant in product formation. The plot of k_{obs} versus 5-NapITP concentration is hyperbolic (Figure 2B), and a fit of the data to the Michaelis−Menten equation yields a k_{pol} value of 27.1 ± 3.8 s^{-1}, a K_D value[3] of 10.3 ± 4.5 μM, and a k_{pol}/K_D of 2.7 × 10^6 M^{-1} s^{-1}. The K_D of 10 μM for 5-NapITP is identical, within experimental error, to that of 14 μM measured for 5-PhITP (*29*) and 2-fold higher than that of 4.6 μM for 5-CE-ITP (*30*), both of which are large (>230 Å^2) and contain significant π-electron density. Likewise, the fast k_{pol} value of ∼27 s^{-1} measured for the incorporation of 5-NapITP opposite an abasic site rivals that of 25 s^{-1} measured with 5-CE-ITP (*30*). However, the value for 5-NapITP is 2-fold slower than the k_{pol} value of 50 s^{-1} measured with 5-PhITP (*29*).

Identical analyses performed with 5-AnITP yield a k_{pol} of 5.3 ± 0.4 s^{-1}, a K_D of 26.5 ± 7.5 μM, and a k_{pol}/K_D of 2.0 × 10^5 M^{-1} s^{-1}. (Data for time courses in product formation as well as the corresponding Michaelis−Menten plot are provided in Supporting Information A.) The overall catalytic efficiency for 5-AnITP is 10-fold lower than that for 5-NapITP and argues that increasing the overall size of the nucleotide has a negative effect on the incorporation opposite the nontemplating DNA lesion. The 10-fold decrease in efficiency results from a combined 2.7-fold decrease in binding affinity (compare 27 μM vs 10 μM for 5-AnITP and 5-NapITP, respectively), in addition to an ∼5-fold reduction in the rate constant for polymerization (compare 5.3 s^{-1} vs 27 s^{-1} for 5-AnITP and 5-NapITP, respectively).

Despite these differences, the collective data set are consistent with our previously proposed model (*30*) in which ground-state binding (K_D values) for a nucleotide opposite an abasic site appears related to the size and desolvation properties of the non-natural nucleotide, whereas the rate of the conformational change (k_{pol}) is linked with the presence of π-electron density. However, the variations in these kinetic parameters also argue that the dynamics of this model are incomplete. In particular, it is surprising that the k_{pol} value

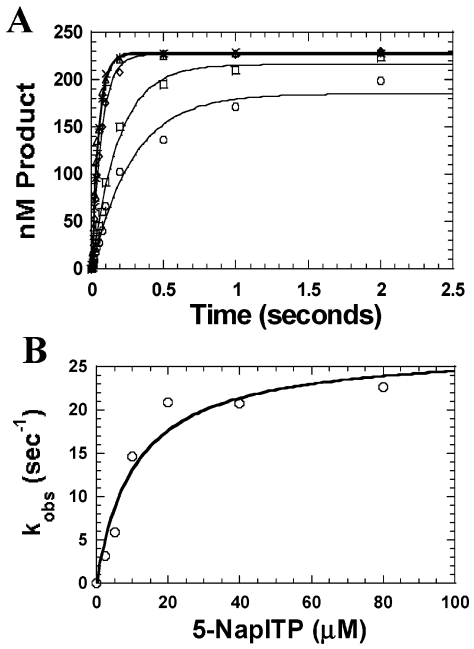

FIGURE 2: (A) Dependency of the apparent burst rate constant on the concentration 5-NapITP as measured under single-turnover conditions. Assays were performed using 1 μM gp43 exo$^-$, 250 nM 13/20 SP, 10 mM $Mg(OAc)_2$, and 5-NapITP in variable concentrations of 2.5 μM (○), 5 μM (□), 10 μM (◇), 20 μM (×), 40 μM (+), and 80 μM (Δ). The solid lines represent the fit of the data to a single exponential. (B) Observed rate constants for incorporation (○) were plotted against 5-NapITP concentration and fit to the Michaelis−Menten equation to determine values corresponding to K_D and k_{pol}.

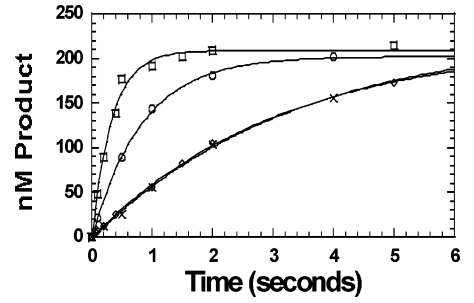

FIGURE 3: Single-turnover time course for the insertion of 5-NapITP (150 μM) opposite the natural nucleotide on the template: A (◇), C (□), G (×), and T (○). Assays were performed using 500 nM gp43 exo$^-$, 250 nM 13/20 mer, 10 mM $Mg(OAc)_2$, and 150 μM 5-NapITP.

[3] Because the reaction was constrained to a single turnover and given that the rate-limiting step for incorporation is likely to be the conformational change preceding phosphoryl transfer (*22*, *29*), the observed Michaelis constant closely approximates a true dissociation constant.

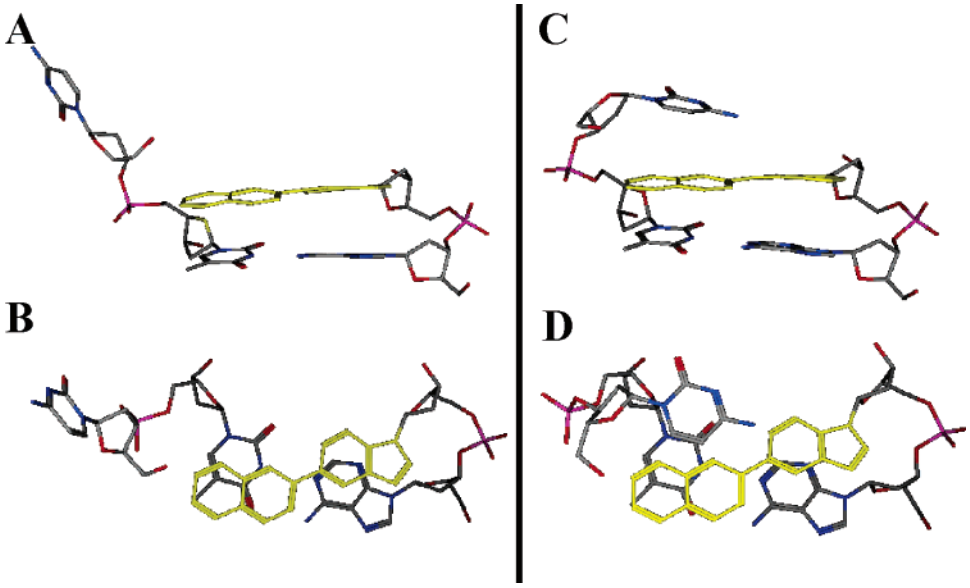

FIGURE 4: Computer generated models for natural and non-natural base pairs generated with 5-napthyl-indole-deoxyribose. All models were generated using Spartan 2004 software. (A) Computer generated model for the structure of 5-napthyl-indole-deoxyribose monophosphate paired opposite thymine in which the natural nucleobase is in an extrahelical conformation. (B) Same as A but with the view of the base pair down the helical axis. (C) Computer generated model for the structure of 5-napthyl-indole-deoxyribose monophosphate paired opposite thymine in which the non-natural nucleobase is stacked with the templating nucleobase in an offset position. (D) Same as C but with the view of the base pair down the helical axis.

for 5-NapITP is actually 2-fold *lower* than that for 5-PhITP because we predicted that a raw increase in π-electron surface area would give rise to a significantly faster k_{pol} value. As pointed out by a reviewer of this article, however, there are at least two reasons why it is unlikely that such a raw increase would yield a better analogue. First, an analogue must also effectively stack against the adjacent primer−template base pair, and second, it must also conform to the geometry of the active site of the protein to be rapidly incorporated. If these criteria are not met, then any excess size could potentially interfere with the closing of the fingers domain and/or alter the configuration of active site geometry to cause the incoming nucleotide to be solvent exposed. Indeed, it is likely that the shear size of naphthalene may reduce the rate of the conformational change step because the surface area of 272.7 Å^2 for 5-napthyl-indole is larger than the active site of the polymerase as estimated from an A−T pair having a surface area of 270.7 Å^2. Consistent with this argument is the fact that the k_{pol} of 5-AnITP is reduced by ~5-fold compared to that of 5-NapITP. In this case, one could argue that the surface area of 319.1 Å^2 for the 5-anthracene-indole is ~50 Å^2 larger than that of the active site of the polymerase. Thus, the overall efficiency of incorporation decreases as the size of the substituent group decreases, despite maintaining a high π-electron surface area.

Kinetic Parameters for Incorporation Opposite Templating Nucleobases. We next tested the ability of gp43 to insert 5-NapITP and 5-AnITP opposite templating DNA. It was predicted that the large size of either analogue would preclude their ability to be incorporated opposite any templating nucleobase. Representative data provided in Figure 3 provides evidence to the contrary as it is clear that 5-NapITP can be incorporated opposite any templating nucleobase. Surprisingly, the data suggest a 10-fold preference for incorporation opposite C and T compared that opposite purines A and G. To further investigate this phenomenon, k_{pol} and K_D values were measured for the incorporation of 5-NapITP opposite templating nucleobases. Data for all time courses in product formation as well as the corresponding Michaelis−Menten plots are provided in Supporting Information B.

Table 1: Summary of Kinetic Rate and Dissociation Constants for the Incorporation of 5-Napthyl-indolyl-2′deoxyriboside Triphosphate (5-NapITP) and 5-Anthracene-indolyl-2′deoxyriboside Triphosphate (5-AnITP) Opposite an Abasic Site and Templating Nucleobases[a]

dXTP	template	k_{pol} (s^{-1})	K_D (μM)	k_{pol}/K_D ($M^{-1}\,s^{-1}$)
5-NapITP	abasic	27.1 ± 1.5	10.3 ± 4.5	2,631,100
5-NapITP	A	0.37 ± 0.03	24.6 ± 8.4	14,800
5-NapITP	C	3.57 ± 0.28	54.8 ± 11.9	65,150
5-NapITP	G	0.41 ± 0.04	17.7 ± 5.7	23,200
5-NapITP	T	2.21 ± 0.40	16.3 ± 7.9	135,600
5-AnITP	abasic	5.3 ± 0.4	26.5 ± 7.5	200,000
5-AnITP	G	0.64 ± 0.12	25.4 ± 9.2	25,200
5-AnITP	T	0.53 ± 0.11	28.5 ± 15.0	18,600

[a] The kinetic parameters, k_{pol}, K_D, and k_{pol}/K_D, were obtained under single-turnover reaction conditions using 1 μM gp43 exo$^-$, 500 nM 13/20SP-mer, and 10 mM Mg^{2+} at varying concentrations of 5-NapITP (5−500 μM) or 5-AnITP (5−500 μM).

As summarized in Table 1, the catalytic efficiency (k_{pol}/K_D) for 5-NapITP incorporation opposite templating DNA is ~20−180-fold lower than that for incorporation opposite an abasic site. In most cases, the lower catalytic efficiency is caused by reductions in each respective k_{pol} value rather than through perturbations in binding affinity because the K_D values measured for 5-NapITP opposite A, G, and T are essentially identical[4]. It is striking that the K_D values of ~20 μM measured opposite these templating bases are only 2-fold higher than that of 10 μM measured for incorporation opposite the abasic site, a lesion devoid of templating information.

[4] As reported in Table 1, a K_D of 55 μM was measured for the incorporation of 5-NapITP opposite C. This value is ~2.5-fold higher than those measured opposite other templating bases. The reason for the difference in binding affinity is unknown.

Scheme 1: Proposed Model for the Enzymatic Incorporation of Non-natural Nucleotides Opposite an Abasic Site or Templating Nucleobases[a]

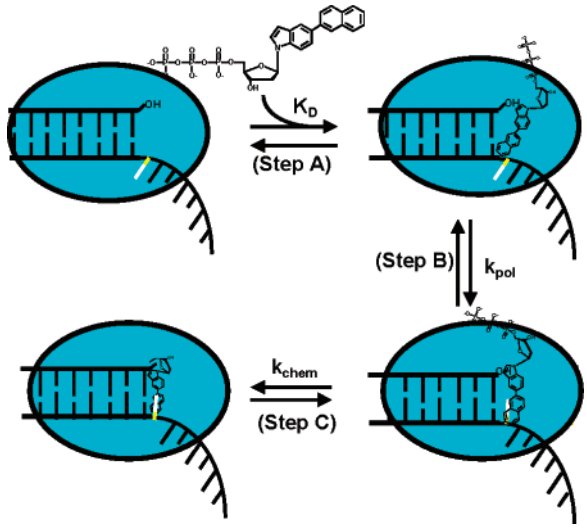

[a] Step A represents the binding of dNTP to the polymerase:DNA complex (K_D). Step B represents the conformational change preceding the phosphoryl transfer (k_{pol}) required to place the triphosphate moiety in close proximity with the positively charged amino acids as well as to stack the nucleobase portion of the incoming dNTP into the hydrophobic environment of the interior of the duplex DNA. Step C represents the phosphoryl transfer step required for elongation of the primer strand (k_{chem}).

As expected, the k_{pol} values for 5-NapITP opposite templating DNA are reduced. However, the 10-fold reduction is not as large as one would predict because of the large size of the analogue. The rationale for this statement is that the k_{pol} for forming a purine−purine mismatch is considerably slower than that for forming a normal Watson−Crick base pair. In the T4 system, for example, the k_{pol} for forming a dA−dA mismatch is 0.029 s^{-1} (*36*; Berdis, A. J., unpublished data) and is >3000 slower than the k_{pol} of 100 s^{-1} measured for forming a normal dT−dA base pair (*22*, *32*). Surprisingly, we do not observe such large differences in k_{pol} values with non-natural nucleotides such as 5-NapITP that contain significant π-electron surface area. We have interpreted this phenomenon within the context of our previously proposed model outlined in Scheme 1 (*30*). An important feature of this model is that the templating nucleobase is proposed to be oriented in an extrahelical position (*38*) that creates a transient void in the DNA (Step A) that functionally mimics an abasic site. It should be noted that the presence an extrahelical templating base has been observed in the structures of various A family polymerases including *Thermus aquaticus* DNA polymerase I (*39*) and the DNA polymerase I fragment from *Bacillus stearothermophilus* (*40*). Although the bacteriophage T4 polymerase is a member of the B family of DNA polymerases, crystallographic evidence from the closely related RB69 DNA polymerase indicates that the templating strand is severely kinked such that the templating base is 11 Å away from the primer−template junction (*41*). This distance precludes direct hydrogen-bonding interactions with the incoming dNTP. However, it does not provide clear evidence for a defined extrahelical conformation as observed with DNA polymerase I (*39*, *40*). Regardless of these differences, our kinetic data does support a mechanism precluding direct interactions with the incoming nucleotide and the templating base because the binding affinities for several non-natural nucleotides, such as 5-NITP, 5-PhITP, and now, 5-NapITP, are essentially identical and independent of templating nucleobase composition (Step A) (*28*−*30*). In contrast to binding affinity, however, the k_{pol} values for these non-natural nucleotides are dependent upon the presence of a templating nucleobase. This suggests that the k_{pol} value represents the rate-limiting conformational change step (Step B) that is required for the proper alignment of the primer−template that then allows for phosphoryl transfer (Step C). When a templating base is present, the rate of this conformational change step is slow (<1 s^{-1} for most analogues) because the shear bulk of the non-natural nucleotide hinders the facile repositioning of the templating nucleobase from the extrahelical position into the interhelical conformation. The rate of this conformational change is faster at an abasic site (>25 s^{-1}) because the lack of a templating nucleobase circumvents the need for this repositioning.

Despite the overall consistencies with this mechanism, it is quite surprising that the k_{pol} values for 5-NapITP vary greatly with the physical composition of the templating nucleobase. In particular, the k_{pol} values opposite the pyrimidines are 10-fold faster than those opposite the purines, a result not observed with other non-natural nucleotides such as 5-PhITP and 5-CE-ITP (*29*, *30*). Furthermore, the apparent inverse correlation between k_{pol} values and the relative size of the templating nucleobase is intriguing. As mentioned previously, the k_{pol} value of ~3 s^{-1} for the incorporation of 5-NapITP opposite pyrimidines is ~10-fold faster than that of ~0.4 s^{-1} measured opposite purines. This trend is also observed when comparing translesion versus normal synthesis because the k_{pol} of 27 s^{-1} for incorporation opposite an abasic site is 10-fold faster than that of ~3 s^{-1} measured opposite the pyrimidines.

At face value, the high catalytic efficiency for incorporation opposite an abasic site can be qualitatively explained by the steric fit model (*42*) because the surface area of 272.7 $Å^2$ for the 5-napthyl-indole−abasic site mispair is nearly identical to that of 270.7 $Å^2$ for an A−T base pair. However, it is unlikely that this mechanism accounts for 5-NapITP incorporation opposite pyrimidines because the size of these formed mispairs would be at least 414 $Å^2$, a size that cannot be accommodated by the tightness of the active site of the DNA polymerase (*42*). Indeed, this size discrepancy makes it even more unlikely that the incoming nucleotide directly pairs with the templating base as suggested by the crystal structure of the RB69 DNA polymerase (*41*) Instead, we envision at least two alternative possibilities that could explain the preferential incorporation of 5-NapITP opposite pyrimidines. The first is that the templating base remains (or is placed) in an extrahelical conformation *after* the incorporation of 5-NapITP (Figure 4A and 4B). In this mechanism, the k_{pol} values are inversely correlated with energetic differences associated with intrahelical stabilization of purines versus pyrimidines. Because pyrimidines have less stacking energies compared to those of purines (*43*−*45*), they are more likely to be stabilized in an extrahelical conformation after nucleotide incorporation. Purines, however, typically prefer to exist in an intrahelical conformation (*43*−*45*). If correct, then the slower rate of the conformational change could reflect the increased energy associated with

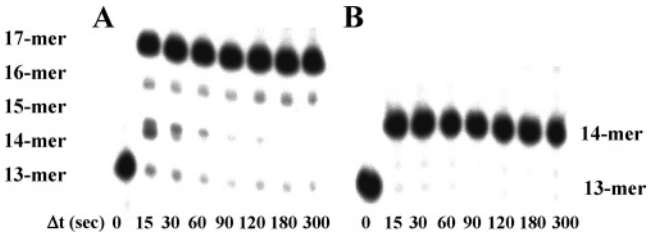

FIGURE 5: 5-NapITP is a chain terminator of translesion synthesis. Assays were performed by pre-incubating the 5′-labeled 13/20 SP-mer (250 nM) with 10 mM $Mg(OAc)_2$, 500 μM dATP, and 1000 μM dGTP in the absence (A) or presence (B) of 25 μM 5-NapITP and initiating the reaction by the addition of 1 μM gp43 exo$^-$. In both cases, the reactions were terminated by the addition of 200 mM EDTA at time intervals ranging from 15 to 300 s. Nucleotide incorporation was analyzed by denaturing gel electrophoresis.

stabilizing purines in an intrahelical position. Indeed, Beuck et al. (*46*) demonstrated that large, polycyclic, non-natural nucleobases can destabilize the intrahelical conformation of the opposing nucleobase and favor its position in an extrahelical conformation. This mechanism is similar to that proposed for the T7 DNA polymerase during the incorporation of pyrene nucleotide opposite a thymine dimer in which the photoproduct is forced out of the active site (*47*). An alternative mechanism, depicted in Figure 4C and D, invokes simple deformation of the newly formed mispair junction through intercalation of the planar aromatic naphthalene moiety into the template strand.

An even more dramatic effect is observed for the incorporation of 5-AnITP opposite T or G. As reported in Table 1, the T4 polymerase incorporates 5-AnITP opposite an abasic site with a 10-fold higher efficiency compared to that opposite templating nucleobases. As was the case with 5-NapITP, the measured binding constants are essentially independent of the templating position (K_D ~30 μM). However, it is striking that the k_{pol} values for incorporation opposite templating positions are only 10-fold slower than that measured opposite the abasic site. In this respect, it is truly remarkable that a high fidelity polymerase such as gp43 can catalyze the enzymatic formation of base pairs that are clearly larger than that predicted to fill the geometry of helical DNA.

5-NapITP Is a Chain Terminator of DNA Synthesis. The chain-termination capabilities of 5-NapITP were quantified by measuring the ability of gp43 exo$^-$ to extend beyond the formed mispair using the previously described experimental protocol (*29*). Briefly, 250 nM DNA was incubated in assay buffer with 10 mM Mg^{2+}, 500 μM dATP, and 1,000 μM dGTP in the absence or presence of 25 μM 5-NapITP. The reaction was initiated by the addition of 1 μM gp43 exo$^-$, and aliquots of the reaction were quenched with 200 mM EDTA at variable times (15−300 s). In the absence of 5-NapITP, gp43 exo$^-$ incorporates natural dNTPs opposite the lesion and then extends beyond the abasic site with modest efficiency (Figure 5A). In the presence of 5-NapTP, however, there is rapid production of the 14-mer, which reflects the exclusive incorporation of the non-natural nucleotide opposite the abasic site (Figure 5B).[5] However, the polymerase cannot elongate beyond the formed mispair

[5] The difference in mobility for DNA containing 5-NapIMP is attributed to the larger size of the naphthalene derivative (~273 Å^2) compared to the nucleobase portion of natural dNMPs (<150 Å^2).

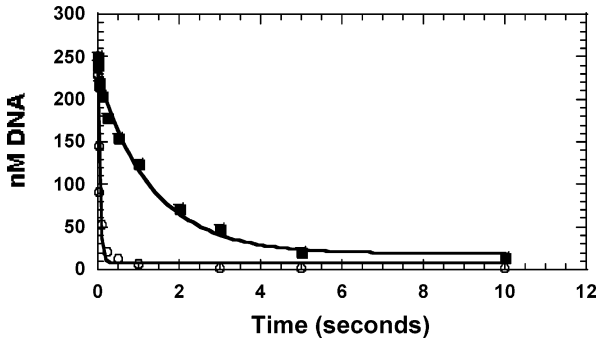

FIGURE 6: Time course in the excision of 5-NapIMP from duplex (■) or single-stranded (○) DNA. The time course in the excision of 5-NapIMP when placed opposite an abasic site was performed by mixing a pre-incubated solution of 1 μM gp43 exo$^+$/10 mM Mg^{2+} vs 250 nM 5′-labeled DNA/10 mM Mg^{2+} (final concentrations) and terminating the reaction at various times by the addition of 350 mM EDTA. The time course in the 5-NapIMP excision from single-stranded DNA was performed under identical conditions. Each time course represents an average of two independent determinations. Time courses were fit to the equation for single-exponential decay, $y = Ae^{-kt} + C$, where A is the burst amplitude, k is the observed rate constant for product formation, and C is the end point of the reaction. The rate constant for the excision of 5-NapIMP from duplex DNA is 0.7 ± 0.1 s^{-1}, whereas that from single-stranded DNA is 20 ± 4 s^{-1}.

because the level of 14-mer remains invariant over the course of the reaction (Δt = 5 min) and, thus, indicates that 5-NapITP is a chain terminator of translesion DNA synthesis. Similar experiments measuring the ability of 5-NapITP to terminate DNA synthesis using unmodified DNA yield an IC_{50} value of ~200 μM (provided in Supporting Information C). These results clearly demonstrate that 5-NapITP is similar to other modified indolyl deoxynucleotides that also act as chain terminators of translesion and normal DNA synthesis (*13*, *35*). The difference in the IC_{50} values for 5-NapITP provides another indication that this analogue is preferentially, but not exclusively, incorporated opposite an abasic site versus templating DNA.

Exonuclease Processing of DNA Containing 5-NapIMP. We previously demonstrated that the excision kinetics of natural and non-natural nucleotides opposite an abasic site were correlated with the relative π-electron surface area of the nucleobase (*13*). Of several analogues tested, 5-PhIMP was excised as the slowest with a low rate constant of ~1 s^{-1} (*13*). This observation predicts that the larger π-electron surface area of 5-napthalene would make it very resistant to degradation from duplex DNA. This hypothesis was tested by measuring the enzymatic hydrolysis of 5-NapIMP when placed opposite an abasic site. Excision reactions were performed in a rapid quench instrument as previously described using single turnover reaction conditions (*13*). The time course in the excision of 5-NapIMP from duplex DNA is best defined as a single-exponential curve (Figure 6), and a fit of the data to eq 3 yields an observed rate constant for excision (k_{exo}) of 0.7 ± 0.1 s^{-1}. This value is ~2- and 20-fold slower than those measured for the excision of 5-PhIMP and 5-NIMP, respectively, and suggests that the enhanced base-stacking ability of 5-NapIMP prevents partitioning of the nucleoside into the exonuclease active site. An alternative explanation, however, is that large base analogues are simply too large to adequately fit into the exonuclease active site. The possibility of steric exclusion was evaluated by compar-

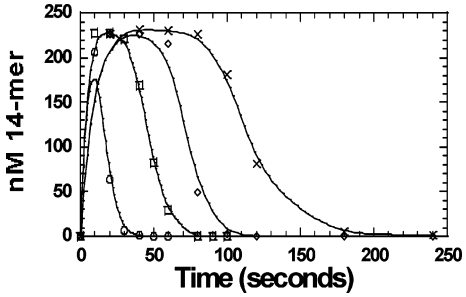

FIGURE 7: Dose dependency of the idle turnover of 5-NapITP opposite an abasic site. gp43 exo$^+$ (1 μM) was added last to a solution containing 250 nM 5′-labeled 13/20SP-mer, 10 mM Mg(OAc)$_2$, 20 μM dATP, and 5-NapITP at the following concentrations: 5 μM (○), 10 μM (□), 15 μM (◇), and 20 μM (×). Reactions were terminated by the addition of 200 mM EDTA at time intervals ranging from 5 to 240 s. Nucleotide incorporation and excision were analyzed by denaturing gel electrophoresis.

ing the kinetics of the excision of single-stranded DNA containing or devoid of 5-NapIMP. A k_{exo} of 20 ± 4 s^{-1} is measured for the degradation of the 14Nap-mer (Figure 6). Although this rate constant is 4-fold slower than the rate constant of 80 s^{-1} measured using unmodified DNA (data not shown), and the value of 20 s^{-1} from single-stranded DNA is >25-fold faster than that from duplex DNA. Thus, the slow rate constant of 0.7 s^{-1} is unlikely to reflect simple steric exclusion from the exonuclease active site. Instead, we propose that the k_{exo} value of 0.7 s^{-1} reflects slow partitioning of the nucleobase into the exonuclease domain from the polymerase active site.

To validate this conclusion, idle-turnover measurements were next performed to measure the overall process of incorporation and excision of the non-natural nucleotide opposite the lesion. During this process, the amount of extension (13-mer to 14-mer) and the subsequent excision (14-mer to 13-mer) can be monitored as a function of time to define rate constants associated with incorporation (k_{pol}) and excision (k_{exo}) (*13*). Time courses in idle turnover were generated using variable concentrations of 5-NapITP (5, 10, 15, and 20 μM). As shown in Figure 7, the attenuation in 14-mer degradation increases as the concentration of 5-NapITP from 5 to 20 μM. These time courses were modeled using global-fit analysis as previously described (*13*) to define values corresponding to K_D, k_{pol}, k_{exo}, and K_D' (the binding affinity of 5-NapITP for incorporation beyond the abasic site). The best fit for all time courses is obtained using the following parameters: K_D = 10 μM, k_{pol} = 27 s^{-1}, k_{exo} = 0.5 s^{-1}, and K_D' = 10 mM. The calculated k_{exo} value of 0.5 s^{-1} from idle-turnover experiments is nearly identical to that of 0.7 s^{-1} measured directly using pre-steady state kinetic techniques. Taken together, these results indicate that nucleotides containing larger π-electron surface areas are more resistant to exonuclease proofreading, a feature consistent with their enhanced base-stacking capabilities rather than simple steric exclusion.

Conclusion. This article outlines the enzymatic characterization of two novel non-natural nucleotide analogues, 5-NapITP and 5-AnITP, that were rationally designed with the goal of achieving exquisite selectivity for incorporation opposite an abasic site. Both analogues contain extensive π-electron surface areas and are incorporated opposite an abasic site with relatively high efficiency. The binding

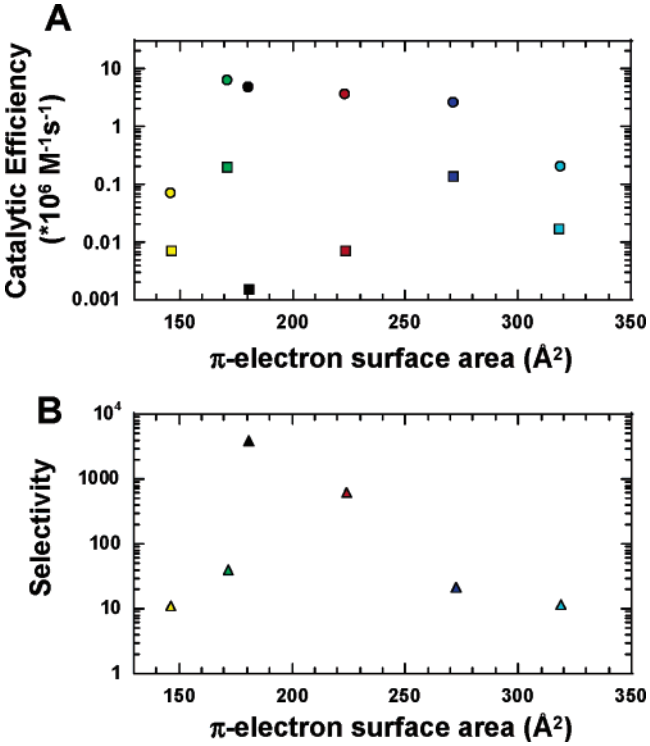

FIGURE 8: (A) Comparison of the catalytic efficiency of incorporation as a function of π-electron surface area. The catalytic efficiencies (k_{pol}/K_D) for incorporation opposite an abasic site are denoted with solid circles (●). The catalytic efficiencies (k_{pol}/K_D) for incorporation opposite T are denoted with solid squares (■). The following color code was used to denote each non-natural nucleotide: yellow = 5-CH-ITP; green = 5-NITP; black = 5-CE-ITP; red = 5-PhITP; blue = 5-NapITP; aqua = 5-AnITP. (B) Comparison of incorporation selectivity as a function of π-electron surface area. Selectivity (▲) is defined as the ratio of catalytic efficiencies (k_{pol}/K_D) for incorporation opposite an abasic site versus incorporation opposite a templating T. The following color code was used to denote each non-natural nucleotide: yellow = 5-CH-ITP; green = 5-NITP; black = 5-CE-ITP; red = 5-PhITP; blue = 5-NapITP; aqua = 5-AnITP.

affinity for both analogues is high as manifest in low K_D values of 10 and 27 μM for 5-NapITP and 5-AnITP, respectively. The low binding constants are consistent with the previously proposed model for translesion DNA synthesis catalyzed by gp43 (*30*) in which the ground-state binding of the incoming nucleotide is driven by its size and desolvation energy. In addition, both analogues have relatively fast k_{pol} values, although the value of 27 s^{-1} measured with the naphthalene analogue is ~5-fold faster than that of 5 s^{-1} measured with the larger anthracene analogue. These data again indicate that the rate constant for polymerization is influenced by the presence of π-electron density (*30*). However, it is clear from the difference in k_{pol} values that size/steric features also play a significant role in modulating the efficiency of translesion DNA synthesis. This point is made clear by inspecting the data in Table 2 and Figure 8A that provide a comprehensive evaluation of the potential role of π-electron surface area for incorporation opposite an abasic site. As seen in both analyses, analogues with the highest catalytic efficiency are those that contain π-electron surface areas between 170 and 275 Å^2. Analogues such as 5-CH-ITP and 5-AnITP, which are below and above this threshold, respectively, have catalytic efficiencies that are reduced by greater than 10-fold. This reduction arises

Table 2: Comparing the Catalytic Efficiency of Incorporation Opposite an Abasic Site or T with π-Electron Surface Area

dXTP	π-electron surface area[a]	catalytic efficiency abasic site ($M^{-1}\,s^{-1}$)	catalytic efficiency templating T ($M^{-1}\,s^{-1}$)	selectivity (abasic/T)[b]
5-CH-ITP[c]	146.17	0.074×10^6	0.007×10^6	10.6
5-NITP[d]	171.43	7.0×10^6	0.19×10^6	36.8
5-CE-ITP[c]	180.71	5.0×10^6	0.0014×10^6	3570
5-PhITP[e]	223.68	3.8×10^6	0.0064×10^6	594
5-NapITP[f]	272.72	2.6×10^6	0.13×10^6	20.2
5-AnITP[f]	319.10	0.2×10^6	0.018×10^6	11.1

[a] π-Electron surface area was calculated using Spartan 2004 software. In all cases, the calculated value represents the surface area of the indole ring in addition to the surface area of the conjugated species of the substituent group. [b] Selectivity is defined as the ratio of catalytic efficiency (k_{pol}/K_D) for incorporation opposite an abasic site to incorporation opposite T. [c] Values taken from Zhang et al. (*30*). [d] Values taken from Reineks and Berdis (*28*). [e] Values taken from Zhang et al. (*29*). [f] This study.

primarily through a decrease in k_{pol} rather than perturbations in K_D values. In the case of 5-CH-ITP, the removal of π-electron density reduces k_{pol} by 50-fold compared to that of the closely related analogue 5-CE-ITP, which contains π-electron density. In the case of 5-AnITP, the reduction in k_{pol} results from an increase in overall size. Collectively, this analysis suggests that one can rationally design an analogue to be efficiently incorporated opposite an abasic site by balancing π-electron surface area with the overall size of the nucleobase.

With this in mind, it was predicted that analogues containing overall large surface areas (greater than 180 Å^2) would be poorly incorporated opposite templating DNA because of steric hindrance. Indeed, large analogues such as 5-CE-ITP and 5-PhITP are incorporated much less efficiently opposite T than opposite the smaller analogue 5-NITP. However, it is very surprising that analogues with excessively large π-electron surface areas such as 5-NapITP and 5-AnITP are less selective than expected. In fact, these analogues are incorporated opposite templating DNA between 100 and 1000-fold more effectively than 5-CE-ITP. At face value, generating selectivity against a templating nucleobase appeared to be an easy task because removing the hydrogen-bonding potential as well as dramatically increasing the size of the nucleobase was predicted to severely retard incorporation opposite any templating nucleobase (*30*). However, these data indicate that simply increasing the size of the substituent group cannot provide selectivity for incorporation opposite damaged versus non-damaged DNA. In fact, Figure 8B provides striking evidence that the selectivity for incorporation (abasic site vs templating T) actually becomes *worse* as the π-electron surface area increases. One hypothesis to explain the loss of selectivity is that the excessive π-electron surface area of 5-NapITP and 5-AnITP has a detrimental effect on the ability of the bacteriophage T4 polymerase to properly discriminate against the incoming nucleotide. In this instance, the energies associated with the larger π-electron surface area and/or lower solvation properties may compensate or even substitute for the energies associated with proper hydrogen-bonding interactions and steric constraints that are needed for incorporation opposite templating DNA. As illustrated in Figure 4, this compensation may result in distorted DNA structures that are stabilized through the enhanced π-electron surface area of the analogue. We emphasize that this mechanism is speculative because it is based solely upon data generated with gp43 as a model. Indeed, it will prove interesting to evaluate if similar trends in selectivity are observed with other DNA polymerases that can utilize these non-natural nucleotides. A particularly attractive system will be to examine various error-prone DNA polymerases such as pol η, pol ι, and pol ζ that display unique structural (*48*−*50*) and biophysical (*51*, *52*) properties compared to high fidelity polymerases such as gp43. Performing a structure−activity relationship of these non-natural nucleotides with error prone DNA polymerases will be prove useful in probing the mechanism by which these polymerases efficiently catalyze translesion DNA synthesis.

SUPPORTING INFORMATION AVAILABLE

Time courses and Michaelis−Menten plot for the incorporation of 5-AnITP opposite an abasic site, time courses and Michaelis−Menten plots for the incorporation of 5-NapITP opposite all natural templating nucleobases, chain termination capabilities of 5-NapITP during normal DNA synthesis, and data for the idle turnover of 5-NapITP opposite an abasic site. This material is available free of charge via the Internet at http://pubs.acs.org.

REFERENCES

1. Switzer, C. Y., Moroney, S. E., and Benner, S. A. (1993) Enzymatic recognition of the base pair between isocytidine and isoguanosine, *Biochemistry 32*, 10489−10496.
2. Malyarchuk, S., Youngblood, R., Landry, A. M., Quillin, E., and Harrison, L. (2003) The mutation frequency of 8-oxo-7,8-dihydroguanine (8-oxodG) situated in a multiply damaged site: comparison of a single and two closely opposed 8-oxodG in *Escherichia coli*, *DNA Repair 11*, 695−705.
3. Suzuki, N., Yasui, M., Geacintov, N. E., Shafirovich, V., and Shibutani, S. (2005) Miscoding events during DNA synthesis past the nitration-damaged base 8-nitroguanine, *Biochemistry 44*, 9238−9245.
4. Xie, Z., Zhang, Y., Guliaev, A. B., Shen, H., Hang, B., Singer, B., and Wang, Z. (2005) The p-benzoquinone DNA adducts derived from benzene are highly mutagenic, *DNA Repair 4*, 1399−13409.
5. Moran, S., Ren, R. X., and Kool, E. T. (1997) A thymidine triphosphate shape analog lacking Watson-Crick pairing ability is replicated with high sequence selectivity, *Proc. Natl. Acad. Sci. U.S.A. 94*, 10506−10511.
6. Matray, T. J., and Kool, E. T. (1999) A specific partner for abasic damage in DNA, *Nature 399*, 704−708.
7. Loeb, L. A. (1991) Mutator phenotype may be required for multistage carcinogenesis, *Cancer Res. 51*, 3075−3079.
8. Starcevic, D., Dalal, S., and Sweasy, J. B. (2004) Is there a link between DNA polymerase beta and cancer? *Cell Cycle 3*, 998−1001.
9. Valko, M., Izakovic, M., Mazur, M., Rhodes, C. J., and Telser, J. (2004) Role of oxygen radicals in DNA damage and cancer incidence, *Mol. Cell. Biochem. 266*, 37−56.
10. Melnikova, V. O., and Ananthaswamy, H. N. (2005) Cellular and molecular events leading to the development of skin cancer, *Mutat. Res. 571*, 91−106.

11. Janatova, M., Zikan, M., Dundr, P., Matous, B., and Pohlreich, P. (2005) Novel somatic mutations in the BRCA1 gene in sporadic breast tumors, *Hum. Mutat. 25*, 319.
12. Wang, Z. (2001) DNA damage-induced mutagenesis: a novel target for cancer prevention, *Mol. Intervention 1*, 269−281.
13. Zhang, X., Lee, I., and Berdis, A. J. (2005) A potential chemotherapeutic strategy for the selective inhibition of promutagenic DNA synthesis by nonnatural nucleotides, *Biochemistry 44*, 13111−13121.
14. Marnett, L. J., and Plastaras, J. P. (2001) Endogenous DNA damage and mutation, *Trends Genet. 17*, 214−221.
15. Haracska, L., Unk, I., Johnson, R. E., Johansson, E., Burgers, P. M., Prakash, S., and Prakash, L. (2001) Roles of yeast DNA polymerases delta and zeta and of Rev1 in the bypass of abasic sites, *Genes Dev. 15*, 945−954.
16. Gibbs, P. E., and Lawrence, C. W. (1995) Novel mutagenic properties of abasic sites in *Saccharomyces cerevisiae*, *J. Mol. Biol. 251*, 229−236.
17. Maor-Shoshani, A., Hayashi, K., Ohmori, H., and Livneh, Z. (2003) Analysis of translesion replication across an abasic site by DNA polymerase IV of *Escherichia coli*, *DNA Repair 2*, 1227−1238.
18. Povirk, L. F., and Shuker, D. E. (1994) DNA damage and mutagenesis induced by nitrogen mustards, *Mutat. Res. 318*, 205−226.
19. Liu, L., and Gerson, S. L. (2004) Therapeutic impact of methoxyamine: blocking repair of abasic sites in the base excision repair pathway, *Curr. Opin. Invest. Drugs 5*, 623−627.
20. Gates, K. S., Nooner, T., and Dutta, S. (2004) Biologically relevant chemical reactions of N7-alkyl-2′deoxyguanosine adducts in DNA, *Chem. Res. Toxicol. 17*, 839−856.
21. Allan, J. M., and Travis, L. B. (2005) Mechanisms of therapy-related carcinogenesis, *Nat. Rev. Cancer 5*, 943−955.
22. Berdis, A. J. (2001) Dynamics of translesion DNA synthesis catalyzed by the bacteriophage T4 exonuclease-deficient DNA polymerase, *Biochemistry 40*, 7180−7191.
23. Shibutani, S., Takeshita, M., and Grollman, A. P. (1997) Translesional synthesis on DNA templates containing a single abasic site. A mechanistic study of the "A rule", *J. Biol. Chem. 272*, 13916−13922.
24. Berthet, N., Roupioz, Y., Constant, J. F., Kotera, M., and Lhomme, J. (1993) Kinetics of deoxyribonucleotide insertion and extension at abasic template lesions in different sequence contexts using HIV-1 reverse transcriptase, *J. Biol. Chem. 268*, 23567−23572.
25. Zhang, Y., Yuan, F., Wu, X., Taylor, J. S., and Wang, Z. (2001) Response of human DNA polymerase iota to DNA lesions, *Nucleic Acids Res. 29*, 928−935.
26. Nelson, J. R., Lawrence, C. W., and Hinkle, D. C. (1996) Deoxycytidyl transferase activity of yeast REV1 protein, *Nature 382*, 729−731.
27. Reineks, E. Z., and Berdis, A. J. (2004) Evaluating the contribution of base stacking during translesion DNA replication, *Biochemistry 43*, 393−404.
28. Zhang, X., Lee, I., and Berdis, A. J. (2005) The use of non-natural nucleotides to probe the contributions of shape complementarity and pi-electron surface area during DNA polymerization, *Biochemistry 44*, 13101−13110.
29. Zhang, X., Zhou, X, Lee, I., and Berdis, A. J. (2005) Hydrophobicity, shape, and π-electron density during translesion DNA synthesis, *J. Am. Chem. Soc. 128*, 143−149.
30. Capson, T. L., Peliska, J. A., Kaboord, B. F., Frey, M. W., Lively, C., Dahlberg, M., and Benkovic, S. J. (1992) Kinetic characterization of the polymerase and exonuclease activities of the gene 43 protein of bacteriophage T4, *Biochemistry 31*, 10984−10994.
31. Frey, M. W., Nossal, N. G., Capson, T. L., and Benkovic, S. J. (1993) Construction and characterization of a bacteriophage T4 DNA polymerase deficient in 3′→5′ exonuclease activity, *Proc. Natl. Acad. Sci. U.S.A. 90*, 2579−2583.
32. Rush, J., and Konigsberg, W. H. (1989) Rapid purification of overexpressed T4 DNA polymerase, *Prep. Biochem. Biotechnol. 19*, 329−340.
33. Yang, Y., and Martin, A. (1992) Synthesis of 5-arylated indoles via palladium-catalyzed cross-coupling reaction of 5-indoleboronic acid with aryl and heteroaryl halides, *Heterocycles 34*, 1395−1398.
34. Zhang, X., Lee, I., and Berdis, A. J. (2004) Evaluating the contributions of desolvation and base-stacking during translesion DNA synthesis, *Org. Biomol. Chem. 2*, 1703−1711.
35. Barshop, B. A., Wren, R. F., and Frieden, C. (1983) Analysis of numerical methods for computer simulation of kinetic processes: development of KINSIM−a flexible, portable system, *Anal. Biochem. 130*, 134−145.
36. Kroutil, L. C., Frey, M. W., Kaboord, B. F., Kunkel, T. A., and Benkovic, S. J. (1998) Effect of accessory proteins on T4 DNA polymerase replication fidelity, *J. Mol. Biol. 278*, 135−146.
37. Patel, P. H., Suzuki, M., Adman, E., Shinkai, A., and Loeb, L. A. (2001) Prokaryotic DNA polymerase I: evolution, structure, and "base flipping" mechanism for nucleotide selection, *J. Mol. Biol. 308*, 823−837.
38. Li, Y., Korolev, S., and Waksman, G. (1998) Crystal structures of open and closed forms of binary and ternary complexes of the large fragment of *Thermus aquaticus* DNA polymerase I: structural basis for nucleotide incorporation, *EMBO J. 17*, 7514−7525.
39. Kiefer, J. R., Mao, C., Braman, J. C., and Beese, L. S. (1998) Visualizing DNA replication in a catalytically active Bacillus DNA polymerase crystal, *Nature 391*, 304−307.
40. Franklin, M. C., Wang, J., and Steitz, T. A. (2001) Structure of the replicating complex of a pol alpha family DNA polymerase, *Cell 105*, 657−667.
41. Kool, E. T. (2002) Active site tightness and substrate fit in DNA replication, *Annu. Rev. Biochem. 71*, 191−219.
42. Hobza, P., and Sponer, J. (2002) Toward true DNA base-stacking energies: MP2, CCSD(T), and complete basis set calculations, *J. Am. Chem. Soc. 124*, 11802−11808.
43. Hunter, C. A. (1993) Sequence-dependent DNA structure. The role of base stacking interactions, *J. Mol. Biol. 230*, 1025−1054
44. Chen, E. C., Chen, E. S., and Wentworth, W. E. (1990) The role of electron donors and acceptors in base stacking in DNA and RNA, *Biochem. Biophys. Res. Commun. 171*, 97−101.
45. Beuck, C., Singh, I., Bhattacharya, A., Hecker, W., Parmar, V. S., Seitz, O., and Weinhold, E. (2003) Polycyclic aromatic DNA-base surrogates: High affinity binding to an adenine-specific base-flipping DNA methyltransferase, *Angew. Chem., Int. Ed. 42*, 3958−3960.
46. Sun, L., Wang, M., Kool, E. T., and Taylor, J. S. (2000) Pyrene nucleotide as a mechanistic probe: evidence for a transient abasic site-like intermediate in the bypass of dipyrimidine photoproducts by T7 DNA polymerase, *Biochemistry 39*, 14603−14610.
47. Ling, H., Boudsocq, F., Woodgate, R., and Yang, W. (2001) Crystal structure of a Y-family DNA polymerase in action: a mechanism for error-prone and lesion-bypass replication, *Cell 107*, 91−102.
48. Silvian, L. F., Toth, E. A., Pham, P., Goodman, M. F., and Ellenberger, T. (2001) Crystal structure of a DinB family error-prone DNA polymerase from *Sulfolobus solfataricus*, *Nat. Struct. Biol. 8*, 984−989.
49. Friedberg, E. C., Fischhaber, P. L., and Kisker, C. (2001) Error-prone DNA polymerases: novel structures and the benefits of infidelity, *Cell 107*, 9−12.
50. Zhang, Y., Yuan, F., Xin, H., Wu, X., Rajpal, D. K., Yang, D., and Wang, Z. (2000) Human DNA polymerase kappa synthesizes DNA with extraordinarily low fidelity, *Nucleic Acids Res. 28*, 4147−4156.
51. Vaisman, A., Frank, E. G., Iwai, S., Ohashi, E., Ohmori, H., Hanaoka, F., and Woodgate, R. (2003) Sequence context-dependent replication of DNA templates containing UV-induced lesions by human DNA polymerase iota, *DNA Repair 2*, 991−1006.
52. Showalter, A. K., Lamarche, B. J., Bakhtina, M., Su, M. I., Tang, K. H., and Tsai, M. D. (2006) Mechanistic comparison of high-fidelity and error-prone DNA polymerases and ligases involved in DNA repair, *Chem. Rev. 106*, 340−360.

BI060418V